IEEE Access
Multidisciplinary ⋮ Rapid Review ⋮ Open Access Journal

Received March 29, 2022, accepted April 4, 2022, date of publication April 7, 2022, date of current version April 14, 2022.

Digital Object Identifier 10.1109/ACCESS.2022.3165653

Reduced-Complexity Decimeter-Level Bluetooth Ranging in Multipath Environments

SHAMMAN NOOR SHOUDHA[1], (Student Member, IEEE), JAYSON P. VAN MARTER[1], (Student Member, IEEE), SHERIEF HELWA[1], (Student Member, IEEE), ANAND G. DABAK[2], (Fellow, IEEE), MURAT TORLAK[1], (Senior Member, IEEE), AND NAOFAL AL-DHAHIR[1], (Fellow, IEEE)

[1]Department of Electrical and Computer Engineering, The University of Texas at Dallas, Richardson, TX 75080, USA
[2]Texas Instruments Inc., Dallas, TX 75243, USA

Corresponding author: Shamman Noor Shoudha (sxn170028@utdallas.edu)

This work was supported by Semiconductor Research Corporation under Grant 2810.076. The work of Murat Torlak (while serving at NSF) was supported by the NSF.

ABSTRACT In this paper, we investigate enhanced super-resolution range estimators with decimeter-level accuracy for multi-antenna and multipath Bluetooth systems. To enhance the traditional MUSIC range estimator for a two-way frequency-hopping Bluetooth channel model, we apply forward-backward averaging and bandwidth extrapolation using Burg's algorithm to improve ranging accuracy, which is limited by the used Bluetooth bandwidth and the quality of the estimated sample covariance matrix. For the multi-antenna case, we compare the Summed Antenna Processing and Individual Antenna Processing methods to process multiple-antenna Bluetooth channel measurements and enhance the range estimation accuracy compared to the single-antenna case. In addition, we investigate a sparsity-aware range estimator which exploits the sparsity of Bluetooth channel impulse response and achieves comparable ranging accuracy to the enhanced MUSIC estimator but at a much lower computational complexity. We apply the greedy Orthogonal Matching Pursuit algorithm to heuristically solve the sparsity-constrained optimization problem for Bluetooth ranging. Furthermore, we evaluate the computational complexity of our investigated Bluetooth range estimators with two complexity-reduction techniques to further reduce the complexity of MUSIC range estimator. Moreover, we analyze the Cramer-Rao Lower Bound (CRLB) on unbiased range estimation using the frequency-hopping Bluetooth channel model and derive a new insightful CRLB expression for a two-path channel model. Finally, we evaluate the Root-Mean-Square Error and Empirical Cumulative Distribution Function performance of our investigated range estimators both on simulated and real-world Bluetooth data that we collected in line-of-sight (LOS) and non-line-of-sight (NLOS) multipath scenarios. Our proposed enhancements on the range estimators improved the ranging accuracy by 58% for our collected Bluetooth data.

INDEX TERMS Reduced complexity, super resolution, ranging, delay estimation, bluetooth, sparse estimator, multipath, decimeter level.

I. INTRODUCTION

Accurate localization is a highly-desired functionality for precise tracking of events, assets, and individuals [1] in Wireless Sensor Networks [2]. A critical initial procedure in localization is determining the distance to an anchor/access point with known location, also known as the ranging procedure. Decimeter-level ranging accuracy enables a plethora of applications such as Internet-of-Things (IoT) positioning [3], autonomous vehicles [4], and crowdsensing [5]. In many of these applications, besides accurate ranging algorithms, low-cost, low-power, and widely available sensors are required for successful deployment. For example, in keyless car entry systems, it is highly desirable to use the mobile phone as a car key.

The main challenges in ranging using Radio Frequency (RF) signals are signal attenuation, multipath propagation, and the limited available bandwidth which degrade localization performance. Current ranging methods based on the Received Signal Strength Indicator (RSSI) do not

The associate editor coordinating the review of this manuscript and approving it for publication was Stefano Scanzio.

offer satisfactory accuracy and security levels to support applications requiring highly accurate localization. For Time-of-Flight (ToF) based ranging methods, precise clock synchronization between the transmitter and receiver is critical for one-way ranging. Moreover, ranging accuracy in ToF-based systems is limited by the available bandwidth. Due to its high market penetration rate and low power consumption, Bluetooth is a popular candidate for localization applications. However, ToF-based Bluetooth distance estimation suffers from a narrow Bluetooth frequency channel bandwidth and timing offsets in one-way ranging. The Multi-Carrier Phase Difference (MCPD) ranging method is able to overcome this bandwidth limitation by collecting channel frequency response (CFR) data over multiple frequencies and it mitigates the coarse clock synchronization problem by working with the two-way instead of one-way channel. Using In-phase/Quadrature (IQ)-samples in MCPD instead of just phase information of the channel measurements has shown robust and superior performance against multipath effects [6].

The Active Reflector (AR)-principle is a well-known method [7], [8] for ranging where two radio transceivers, called the Initiator and the Reflector, send and receive constant tone signals over multiple frequencies. Different range estimators, such as gradient-based [9], Fourier-transform-based [10] and super-resolution-based [6] approaches are then applied to extract the range information from multi-frequency channel measurements. These range estimators model the channel impulse response (CIR) as a superposition of multipath components (MPCs) defined by their complex magnitudes, angles-of-arrival (AoAs), and ToFs. The distance between the Initiator and Reflector to be estimated $\hat{d}$ is directly related to the estimated ToF $\hat{\tau}$ of the line-of-sight (LOS) path as follows

$$\hat{d} = c\hat{\tau}. \tag{1}$$

Therefore, the range estimator accuracy depends on how accurately the ToF of the LOS path is being estimated. The range estimator should be able to estimate the CIR and resolve the MPCs by estimating their parameters and the LOS path distance. Typically, the resolution of the distance estimator is limited by the inverse of the transmission bandwidth. The low resolution resulting from small bandwidth limits the ability to resolve closely-spaced MPCs which leads to a low ranging accuracy and biased estimators [11].

The gradient-based approach utilizes the slope of CFR phase data, which depends on the LOS ToF, to estimate the range, as shown in [9]. However, in the presence of multipath, the gradient-based approach performs poorly as the phase information tends to over-estimate the range. The Inverse Fast Fourier Transform (IFFT)-based approach reconstructs the CIR from CFR data using the IFFT. This method achieves better performance than the gradient-based approach in multipath scenarios. However, in non-line-of-sight (NLOS) scenarios where the direct LOS path is obstructed, the IFFT method suffers from low accuracy.

For ranging, the channel estimation problem can be formulated as a delay estimation problem in the frequency domain. Hence, the ranging problem becomes a parameter estimation problem of superimposed complex exponentials which are the MPCs of the CIR. When formulated as a delay estimation problem, the ranging problem can be considered a classical array signal processing problem, where MUSIC [12], ESPIRIT [13], and Matrix Pencil [14] estimators are applicable. In [6], MUSIC is applied for ranging based on single-snapshot one-way channel measurements, where spatial smoothing is applied to form a Hankel matrix from the CFR [15]. However, this work assumed the single-antenna case and no enhancements were applied to improve the MUSIC estimator performance.

The typically sparse nature of the CIR MPCs can be exploited to apply sparsity-aware estimators [16] for ranging. The MPCs are confined to a finite grid of candidate ToFs. Since the sparse estimator works directly on the CFR measurements, subspace (signal or noise) estimation is not required, unlike the MUSIC algorithm. To mitigate the well-known basis mismatch error problem in sparse estimators, gridless versions of the sparse estimators have been proposed [17]. However, the iterative gridless sparse estimators have high computational complexity which increases rapidly with an increasing number of MPCs. Using greedy algorithms such as Orthogonal Matching Pursuit (OMP), the sparse optimization problem can be solved with much lower complexity than subspace-based estimators. Table 1 illustrates the comparison of this work with the existing Bluetooth range estimators in the literature.

The main contributions of this paper are

- We carried out a real-world Bluetooth data collection campaign using Bluetooth multi-antenna boards in anechoic chamber and parking lot environments, for LOS and NLOS multipath scenarios, and single/multiple-antenna configurations.
- We propose an enhanced super-resolution MUSIC-based range estimator which carefully integrates smoothing, forward-backward sample covariance matrix averaging, bandwidth extrapolation, and multi-antenna combining. Forward-backward averaging improves the sample covariance matrix estimate, bandwidth extrapolation virtually extends the limited Bluetooth bandwidth, and multi-antenna combining leverages spatial diversity to improve ranging accuracy.
- We propose a low-complexity sparsity-aware range estimator based on the OMP greedy algorithm. In addition, we apply two complexity reduction methods for the MUSIC range estimator; namely, the signal-subspace-based estimator and the Lanczos algorithm to approximate the sample covariance matrix eigenvectors. We compare the computational complexity, measured in terms of the number of complex multiplications, of the MUSIC and the OMP-based sparse estimators with and without our proposed enhancements.

- We evaluate the Empirical Cumulative Distribution Function (ECDF) and the Root Mean Square Error (RMSE) performances of the enhanced MUSIC and sparse estimators and show that our proposed enhancements to the MUSIC and sparse estimators can improve the Bluetooth ranging accuracy significantly. In addition, we demonstrate that the sparse OMP estimator and the enhanced MUSIC estimator have comparable performance, while the former has much lower complexity than the latter. Moreover, the proposed complexity reduction methods do not degrade the MUSIC performance appreciably.
- We analyze the Cramer-Rao Lower Bound on the variance of any unbiased range estimator in a multipath channel, evaluate it for real-world Bluetooth measurements, and compare it with the investigated MUSIC and OMP range estimators. To gain further insights, we derive a new closed-form CRLB expression for the special case of a two-path CIR as a function of the number and width of the Bluetooth frequency channels and the time separation between the two CIR paths.

The rest of this paper is organized as follows: In Section II, we present the two-way channel model for multi-antenna Initiator-Reflector-based ranging and briefly review the gradient, IFFT, and MUSIC estimators. In Section IV, we describe the sparsity-aware range estimator based on the greedy OMP algorithm. Section V proposes enhancements to the super-resolution MUSIC algorithm, which are followed by complexity reduction methods in Section VI. Sections VII and VIII present our real-world Bluetooth data collection campaign and numerical results of the proposed estimators on both simulated and collected data, respectively. Finally, Section IX concludes the paper, and both MUSIC spectrum and CRLB derivations are given in Appendices A and B, respectively.

Notation: We denote matrices with bold-face upper case and vectors with bold-face lowercase letters. The transpose, complex-conjugate and complex-conjugate transpose operators are denoted as $(\cdot)^T$, $(\cdot)^*$, and $(\cdot)^H$, respectively. $\Re[\cdot]$ and $\Im[\cdot]$ denote the real and imaginary parts of a complex number, respectively. The subscripts $(\cdot)_M$, $(\cdot)_p$, $(\cdot)_t$, $(\cdot)_f$ denote Initiator ($M = I$) or Reflector ($M = R$), pth path, time-domain and frequency-domain quantities, respectively. The superscript $(\cdot)^l$ refers to the lth antenna measurement. $\mathbb{C}^{M\times N}$ and $\mathbb{R}^{M\times N}$ denote the set of all $M \times N$ complex and real matrices, respectively. $\odot$ is the Hadarmard (element-wise) product and $(\cdot)^{\circ 2}$ is the element-wise square operation. $\|\cdot\|_0$, $\|\cdot\|_2$, $\mathbf{I}_N$, and $\mathbf{J}_N$ denote the norm-0, norm-2 of a vector, $N \times N$ identity matrix, and exchange matrix, respectively. Key variables and acronyms used in the paper are summarized in Tables 2 and 3, respectively.

II. SYSTEM MODEL AND ASSUMPTIONS

In this section, we describe our investigated ranging scenario, develop the system model and state our assumptions. To be relevant to the current Bluetooth standards, we consider a ranging system that uses frequency hopping over multiple frequency channels to collect multi-channel CFR measurements. We consider a two-way ranging system utilizing the AR-principle [10] because it eliminates the effects of the unknown phase offset between the transmitter and receiver in one-way ranging. We apply the AR-ranging method in the IQ-domain since the magnitude information also contains useful channel information [6] in addition to the phase information. Following the AR-principle, two roles are defined, namely Initiator (I) and Reflector (R). The I and R nodes will first agree upon a pseudo-random channel hopping sequence as part of the initiation handshake procedure. After the handshake, they exchange tone signals on these agreed-upon frequencies in the I/Q measurement stage. The Initiator first transmits a constant tone signal at frequency f_k. Upon receiving this signal, the Reflector performs an I/Q measurement which depends on the Initiator and Reflector's local oscillators and the distance between them. Then, the Reflector sends back a constant tone signal at the same frequency f_k and the Initiator performs an I/Q measurement. The Initiator and Reflector perform constant tone signal transmission and reception over the entire available frequency band to increase measurement bandwidth. After this procedure is completed for all hopping frequencies, the Reflector sends the measurements to the Initiator for range estimation. Next, we formulate the generalized multi-channel, multi-antenna, and multi-path system model for AR-ranging.

To develop the two-way multi-antenna frequency hopping channel model, we assume that the received signal at the Initiator/Reflector for antenna l and frequency channel f_k has the form

$$y_M^{(l)}(k) = \sum_{p=0}^{P-1} \alpha_{p,M}^{(l)} e^{j\phi_M^{(l)}(k,\tau_p)} + w_M^{(l)}(k), \quad k = 0, \ldots, K-1; \quad l = 1, \ldots, L_M, \tag{2}$$

where K denotes the number of frequency channels, L_M is the number of antennas at the Initiator/Reflector, P is the total number of paths, $\{\alpha_{p,M}^{(l)}\}$ and $\{\phi_M^{(l)}(k, \tau_p)\}$ are the amplitudes and phases of the p^{th} path at the l^{th} antenna, respectively, τ_p is the ToF of the p^{th} path, $w_M^{(l)}(k)$ is the additive noise term (assumed white and Gaussian) for the l^{th} antenna and the kth frequency. In addition, we define Δ_f to be the frequency step size, $\Delta_t^{(l)}$ as the time-offset between the Initiator and the Reflector at the lth antenna, and θ as the phase difference between the local oscillators of the Initiator and the Reflector. We can write the phase of the received signal at the Initiator as

$$\phi_I^{(l)}(k, \tau_p) = -2\pi k \Delta_f (\tau_p - \Delta_t^{(l)}) - \theta, \tag{3}$$

and at the Reflector as

$$\phi_R^{(l)}(k, \tau_p) = -2\pi k \Delta_f (\tau_p + \Delta_t^{(l)}) + \theta. \tag{4}$$

TABLE 1. Comparison of this work with existing bluetooth range estimators.

Comparison Aspect	Scenario	Boer *et. al.* [6]	Zand *et. al.* [8]	Gunia *et. al.* [9]	Yang *et. al.* [18]	This work
Channel Model	Two-way channel		✓	✓		✓
	One-way channel	✓			✓	
Estimator	RSSI based				✓	
	Phase based		✓	✓		
	FFT based			✓		
	MUSIC	✓				✓
	Enhancements on MUSIC					✓
	Sparse					✓
	Enhancements on Sparse					✓
Multi-antenna combining	-	✓				✓
Multipath scenario	Line-of-Sight	✓	✓	✓		✓
	Non Line-of-Sight	✓			✓	✓

TABLE 2. List of key variables.

Symbol	Description	Symbol	Description
Δ_f	Spacing between two adjacent frequencies	$\mathbf{y}_T^{(l)} \in \mathbb{C}^{K\times 1}$	Two-way CFR vector for lth antenna
M	Operation mode of the node, Initiator ($M = I$) or Reflector ($M = R$)	$\mathbf{C} \in \mathbb{C}^{(m+1)\times(K-m)}$	Hankel matrix formed using two-way CFR
K	Number of frequency channels	$\hat{\mathbf{R}} \in \mathbb{C}^{(m+1)\times(m+1)}$	Sample covariance matrix
P	Number of multipaths	q	Estimated number of sources
L_I or L_R	Number of antennas at Initiator or Reflector	$\mathbf{U}_q \in \mathbb{C}^{(m+1)\times q}$	Matrix with signal eigenvectors as columns
$y_I^{(l)}(k)$ or $y_R^{(l)}(k)$	kth frequency of lth antenna one-way channel frequency response (CFR) at Initiator or Reflector	$\mathbf{U}_n \in \mathbb{C}^{(m+1)\times(m-q+1)}$	Matrix with noise eigenvectors as columns
τ_p	Time-of-flight of pth path	$\mathbf{\Lambda}(\lambda_q) \in \mathbb{R}^{q\times q}$	Diagonal matrix with signal subspace eigenvalues as diagonal elements
$\Delta_t^{(l)}$	Timing offset between Initiator and Reflector at lth antenna	$\mathbf{\Lambda}(\lambda_n) \in \mathbb{R}^{(m-q+1)\times(m-q+1)}$	Diagonal matrix with noise subspace eigenvalues as diagonal elements
$\alpha_{p,M}^{(l)}$	Magnitude of pth multipath at lth antenna for Initiator ($M = I$) or Reflector ($M = R$)	$\Phi^m(\tau) \in \mathbb{C}^{(m+1)\times 1}$	Steering vector for time-of-flight τ
$\phi_I^{(l)}(k,\tau_p)$ or $\phi_R^{(l)}(k,\tau_p)$	Phase of kth frequency and pth multipath for lth antenna at Initiator or Reflector	$\mathbf{H}_I^{(l)}$ or $\mathbf{H}_R^{(l)} \in \mathbb{C}^{K\times P}$	Two-way channel matrix for lth antenna at Initiator or Reflector
$w_I^{(l)}(k)$ or $w_R^{(l)}(k)$	Noise at kth frequency for lth antenna at Initiator or Reflector	c	Speed of light in vacuum
m	Spatial smoothing filter length	$\hat{d}$	Estimated distance

Using the above two equations, we can re-write the Initiator and Reflector signals as

$$y_I^{(l)}(k) = h_I^{(l)}(k)e^{j\psi_{p,I}^{(l)}(k)} + w_I^{(l)}(k), \tag{5}$$

$$y_R^{(l)}(k) = h_R^{(l)}(k)e^{-j\psi_{p,R}^{(l)}(k)} + w_R^{(l)}(k), \tag{6}$$

where, $h_I^{(l)}(k) = \sum_{p=0}^{P-1} \alpha_{p,I}^{(l)} e^{-j2\pi k\Delta_f \tau_p}$, and $h_R^{(l)} = \sum_{p=0}^{P-1} \alpha_{p,R}^{(l)} e^{-j2\pi k\Delta_f \tau_p}$ are the multi-path channels at the Initiator and Reflector, respectively, $\psi_{p,I}^{(l)}(k) = 2\pi k\Delta_f \Delta_t^{(l)} - \theta$, and $\psi_{p,R}^{(l)}(k) = -2\pi k\Delta_f \Delta_t^{(l)} + \theta$. Equations (5) and (6) can also be expressed in matrix forms as follows. We stack the multiple paths as columns of the channel matrix $\mathbf{H}^{(l)} \in \mathbb{C}^{K\times P}$ (for simplicity, the Initiator/Reflector subscript is dropped). The signal magnitudes and phases are stacked in a column vector $\mathbf{x}^{(l)} \in \mathbb{C}^{P\times 1}$. Finally, we concatenate the CFRs to form $\mathbf{y}^{(l)} \in \mathbb{C}^{K\times 1}$ which can be written as

$$\mathbf{y}^{(l)} = \mathbf{H}^{(l)}\mathbf{x}^{(l)} + \mathbf{w}^{(l)}, \tag{7}$$

where we used the following definitions

$$\mathbf{y}^{(l)} = [y^{(l)}(0), y^{(l)}(1), \ldots, y^{(l)}(K-1)]^T, \tag{8}$$

$$\mathbf{x}^{(l)} = [\alpha_1^{(l)}e^{j\psi_1^{(l)}}, \alpha_2^{(l)}e^{j\psi_2^{(l)}}, \ldots, \alpha_P^{(l)}e^{j\psi_P^{(l)}}]^T, \tag{9}$$

$$\mathbf{w}^{(l)} = [w^{(l)}(0), w^{(l)}(1), \ \ldots \ , w^{(l)}(K-1)]^T, \tag{10}$$

$$\mathbf{H}^{(l)} = [\boldsymbol{\gamma}(\tau_1), \boldsymbol{\gamma}(\tau_2), \ldots, \boldsymbol{\gamma}(\tau_P)], \tag{11}$$

$$\boldsymbol{\gamma}(\tau_p) = [1, e^{-j2\pi\Delta_f\tau_p}, \ldots, e^{-j2\pi(K-1)\Delta_f\tau_p}]^T. \tag{12}$$

Here, $\mathbf{H}^{(l)}$ is the array manifold matrix with $\boldsymbol{\gamma}(\tau_p)$'s as the steering vectors. We can now find the two-way CFR for the l^{th} antenna and K frequencies by multiplying the received signals at the Initiator and Reflector. If we assume a stationary

TABLE 3. Key acronyms.

Acronym	Fullform
AR	Active Reflector
BLE	Bluetooth Low Energy
BWE	Bandwidth Extrapolation
CFR	Channel Frequency Response
CRLB	Cramer-Rao Lower Bound
ECDF	Empirical Cumulative Distribution Function
EVD	Eigenvalue Decomposition
FB	Forward-Backward
IAP	Individual Antenna Processing
IFFT	Inverse Fast Fourier Transform
LOS	Line-of-Sight
MPC	Multi Path Component
MUSIC	MUltiple SIgnal Classification
NLOS	Non Line-of-Sight
OMP	Orthogonal Matching Pursuit
RMSE	Root-Mean-Square Error
SAP	Summed Antenna Processing
SVD	Singular Value Decomposition
ToF	Time of Flight

channel without noise, the one-way channels outputs are $\mathbf{H}_I^{(l)}\mathbf{x}_I^{(l)} = \mathbf{H}_R^{(l)}\mathbf{x}_R^{(l)} = \mathbf{H}_O^{(l)}\mathbf{x}^{(l)}$. We find the two-way CFR by taking the Hadamard product of the Initiator and Reflector CFRs to get

$$\mathbf{y}_T^{(l)} = \mathbf{y}_I^{(l)} \odot \mathbf{y}_R^{(l)} = \mathbf{H}_I^{(l)}\mathbf{x}_I^{(l)} \odot \mathbf{H}_R^{(l)}\mathbf{x}_R^{(l)} = \{\mathbf{H}_O^{(l)}\mathbf{x}^{(l)}\}^{\circ 2}. \quad (13)$$

Our aim is to estimate the LOS component from $\mathbf{y}_T^{(l)} = [y_T^{(l)}(0), y_T^{(l)}(1), \ldots, y_T^{(l)}(K-1)]^T \in \mathbb{C}^{K\times 1}$, where τ_0 denotes the delay of the LOS path.

III. TRADITIONAL RANGE ESTIMATORS

In this section, we review three widely-used ranging approaches from the two-way CFR; namely, gradient-based, IFFT-based, and MUSIC-based approaches.

In the gradient-based ranging approach, only the phase information of the two-way channel is utilized. In the noiseless single-path case, if the ToF is τ_1 with gain α_1, we can readily verify that the two-way channel becomes

$$\mathbf{y}_T = (\boldsymbol{\gamma}(\tau_1)\alpha_1)^2 = (\alpha_1)^2 \begin{bmatrix} 1 \\ e^{-j2\pi\Delta_f 2\tau_1} \\ \vdots \\ e^{-j2\pi(K-1)\Delta_f 2\tau_1} \end{bmatrix}. \quad (14)$$

The phase differences of the two-way channel $\mathbf{y}_T$ at two adjacent frequencies k and $k+1$, with proper normalization, will give the range information. The final range, $\hat{d}$, can be estimated as an average of all the range estimates from each pair of frequencies, i.e.

$$\hat{d} = \frac{c}{4\pi(K-1)} \sum_{k=0}^{K-2} \frac{\angle y_T(k) - \angle y_T(k+1)}{\Delta_f}. \quad (15)$$

The performance of the gradient-based ranging approach suffers from multipath effects. Moreover, for larger values of LOS distance, measurement errors have a stronger impact on the estimated range [9].

An alternative to the gradient-based approach is the IFFT-based approach which utilizes both the magnitude and phase information of the CFR data. Starting with the CIR expression (Initiator or Reflector)

$$h^{(l)}(k) = \sum_{p=0}^{P-1} \alpha_p^{(l)} e^{-j2\pi k\Delta_f \tau_p}. \quad (16)$$

Since the frequency spacing is uniform for $h^{(l)}(k)$, a simple IFFT operation separates the multipaths, limited by a time resolution determined by the inverse of the utilized bandwidth, and provides the propagation delays of these paths [19]. The IFFT approach outperforms the gradient-based approach in multipath environments. However, the resolutions offered by the gradient or IFFT-based approaches can be further improved by applying super-resolution-based range estimators which we will discuss next.

The measured CFR has a uniform frequency sampling grid. Therefore, we can form a Hankel matrix from the CFR with smoothing parameter $1 \le m < K$ as follows

$$\mathbf{C} = \begin{bmatrix} y_T^{(l)}(0) & y_T^{(l)}(1) & \ldots & y_T^{(l)}(K-m-1) \\ y_T^{(l)}(1) & y_T^{(l)}(2) & \ldots & y_T^{(l)}(k-m) \\ \vdots & \vdots & & \vdots \\ y_T^{(l)}(m) & y_T^{(l)}(m+1) & \ldots & y_T^{(l)}(K-1) \end{bmatrix}, \quad (17)$$

which admits a Vandermonde decomposition [20] and allows us to apply the super-resolution MUSIC algorithm for ToF estimation. We can either apply Singular Value Decomposition (SVD) on the Hankel matrix $\mathbf{C} \in \mathbb{C}^{(m+1)\times(K-m)}$, or Eigenvalue Decomposition (EVD) on the sample covariance matrix $\hat{\mathbf{R}} \in \mathbb{C}^{(m+1)\times(m+1)}$ to separate the signal and noise subspaces as follows

$$\begin{aligned} \hat{\mathbf{R}} &= \frac{\mathbf{C}\mathbf{C}^H}{(K-m)} \\ &= \begin{bmatrix} \mathbf{U}_q & \mathbf{U}_n \end{bmatrix} \begin{bmatrix} \Lambda(\lambda_\mathbf{q}) & 0 \\ 0 & \Lambda(\lambda_\mathbf{n}) \end{bmatrix} \begin{bmatrix} \mathbf{U}_q^H \\ \mathbf{U}_n^H \end{bmatrix}. \end{aligned} \quad (18)$$

The orthonormal matrices $\mathbf{U}_q \in \mathbb{C}^{(m+1)\times q}$ and $\mathbf{U}_n \in \mathbb{C}^{(m+1)\times(m-q+1)}$ contain the signal and noise eigenvectors as columns, respectively, and q is the estimated number of signal sources (signal subspace dimension). The diagonal matrices $\boldsymbol{\Lambda}(\lambda_q) \in \mathbb{R}^{q\times q}$ and $\boldsymbol{\Lambda}(\lambda_n) \in \mathbb{R}^{(m-q+1)\times(m-q+1)}$ contain the signal and noise eigenvalues, respectively.

The number of signal sources q can be estimated using the popular Minimum Description Length (MDL) or Akaike Information Criterion (AIC) [21]. After performing the EVD and selecting the signal and noise eigenvectors, we can estimate the delay of the LOS path by selecting the first peak of the following MUSIC pseudo-spectrum

$$J(\tau) = \frac{1}{\left\|\mathbf{U}_n^H \Phi^m(\tau)\right\|_2^2}, \quad (19)$$

where $\Phi^m(\tau) = [1, e^{-j2\pi\Delta_f\tau}, e^{-j2\pi 2\Delta_f\tau}, \ldots, e^{-j2\pi m\Delta_f\tau}]$. After extracting the ToF of the LOS path, we multiply it by the

speed of light to compute the distance between the Initiator and the Reflector. The two-way CFR is more sensitive to multipath effects than the one-way CFR since the number of multipaths is increased from p to $2p-1$ in the former due to cross products that degrade LOS estimation.

IV. SPARSITY-AWARE RANGE ESTIMATOR

The MUSIC range estimator requires calculation of the sample covariance matrix and its computationally-intense EVD. In this section, we present a sparsity-aware range estimator which does not require this EVD.

A. SPARSE RECOVERY FORMULATION OF THE RANGING PROBLEM AND KEY ASSUMPTIONS

The ToF of LOS path estimation problem from the CFRs of (7) can be formulated as a sparse optimization problem as follows [16]. First, we define a search range of interest for the ToF estimation as

$$\bar{\tau} = [\tau_1, \tau_2, \ldots, \tau_N], \tag{20}$$

where $N \gg P$ is the number of uniformly-distributed candidate ToFs. Using this search grid, we construct an overcomplete array manifold matrix $\Psi \in \mathbf{C}^{K\times N}$ whose columns are steering vectors for each of the ToFs in $\bar{\tau}$, i.e.

$$\Psi = \frac{1}{\sqrt{N}}[\boldsymbol{\gamma}(\tau_1), \boldsymbol{\gamma}(\tau_2), \ldots, \boldsymbol{\gamma}(\tau_N)]. \tag{21}$$

Using the overcomplete array manifold matrix Ψ, we can write the received CFR in (7) as follows

$$\mathbf{y}^{(l)} = \Psi \mathbf{s}^{(l)} + \mathbf{w}^{(l)}, \tag{22}$$

where $\mathbf{s}^{(l)} = [s_1^{(l)}, s_2^{(l)}, \ldots, s_N^{(l)}]^T \in \mathbb{C}^{N\times 1}$ contains the signal components for the l^{th} antenna corresponding to all N possible ToFs in the search grid. Since the number of true paths P is much smaller than the number of search grid points N, $\mathbf{s}^{(l)}$ becomes a sparse vector with P non-zero components and the remaining $N-P$ components are close to zero. To recover the P-sparse signal component vector $\mathbf{s}$ (superscript l is dropped for simplicity), we solve the following l_0-norm minimization problem in the absence of noise

$$\min_{\mathbf{s}} \|\mathbf{y} - \Psi\mathbf{s}\|_2^2 \quad s.t.\ \|\mathbf{s}\|_0 \le \eta, \tag{23}$$

where η is the constraint on the maximum sparsity level of $\mathbf{s}$. However, the l_0-norm optimization problem in (23) is NP-hard to solve. In the literature, many methods and algorithms have been proposed for sparse signal recovery including convex relaxation or l_1 optimization [22], l_q, $0 < q < 1$ norm optimization [23], Iterative Hard Thresholding (IHT) [24], Compressive Sampling Matching Pursuit (CoSaMP) [25], Maximum Likelihood Estimation (MLE), etc. Here, we apply a popular greedy algorithm, namely the orthogonal matching pursuit (OMP) [26], to iteratively solve the l_0-norm optimization problem in (23).

B. ORTHOGONAL MATCHING PURSUIT (OMP)

The OMP algorithm belongs to the class of matching or "greedy" pursuit algorithms for sparse signal recovery. The major advantages of the OMP algorithm are its low computational complexity and ease of implementation. In our sparse recovery problem (23), $\mathbf{s}$ has a maximum of η non-zero components (remaining components are close to zero). Therefore, in the noiseless case, the CFR $\mathbf{y}$ can be considered as a linear combination of η columns of Ψ. To identify the sparse signal $\mathbf{s}$, OMP selects columns of Ψ whose linear combination best matches the CFR $\mathbf{y}$ in a greedy manner. More specifically, at each iteration, the OMP algorithm selects the column of Ψ that is most strongly correlated with $\mathbf{y}$. Then, the contribution of this column of Ψ is subtracted from $\mathbf{y}$ in the next step and the same steps are applied to the updated Ψ and $\mathbf{y}$. After η iterations, OMP finds η columns from Ψ whose indices represent the locations of the MPCs. After finding the ToFs of the MPCs, their magnitudes can be easily calculated using the least squares method. The steps of the OMP algorithm for range estimation are given in Algorithm (1). The estimate $\hat{\mathbf{s}}$ has non-zero components at the indices contained in $\boldsymbol{\Lambda}_\eta$. The j^{th} value of $\mathbf{x}_t$ denotes the λ_j^{th} component of $\hat{\mathbf{s}}$.

Algorithm 1: OMP Range Estimation

Data: $\mathbf{y}$, $\boldsymbol{\Psi}$, η, $\bar{\tau}$
Result: estimate of ideal signal $\hat{\mathbf{s}}$, τ_0
$\mathbf{r}_0 \leftarrow \mathbf{y}$;
$\boldsymbol{\Lambda}_0 \leftarrow \emptyset$;
$\boldsymbol{\Phi}_0 \leftarrow \emptyset$;
$t \leftarrow 1$;
while $t \le \eta$ **do**
  $\lambda_t = \arg\max_j |\langle \mathbf{r}_0, \boldsymbol{\Psi}_j \rangle|$;
  $\boldsymbol{\Lambda}_t = \boldsymbol{\Lambda}_{t-1} \bigcup \lambda_t$ and $\boldsymbol{\Phi}_t = [\boldsymbol{\Phi}_{t-1} \boldsymbol{\Psi}_{\lambda_t}]$;
  $\mathbf{x}_t = \arg\min_x \|\mathbf{y} - \boldsymbol{\Phi}_t \mathbf{x}\|_2^2$;
  $\mathbf{a}_t = \boldsymbol{\Phi}_t \mathbf{x}_t$ and $\mathbf{r}_t = \mathbf{y} - \mathbf{a}_t$;
  $t \leftarrow t + 1$;
end
$\tau_0 \leftarrow \bar{\tau}(\min(\boldsymbol{\Lambda}_\eta))$;

V. ENHANCED RANGE ESTIMATION

In this section, we present three enhancements to the super-resolution MUSIC and sparsity aware range estimators, namely forward-backward averaging, bandwidth extrapolation, and multi-antenna combining. All of these enhancements can be applied to the MUSIC range estimator while only the latter two are applicable to the OMP algorithm.

A. FORWARD-BACKWARD AVERAGING

The super-resolution MUSIC range estimator finds the LOS ToF from the received sample covariance matrix $\hat{\mathbf{R}}$ of the CFR. Using the smoothing length $1 \le m < K$, we express

the sample covariance matrix as follows

$$\hat{\mathbf{R}} = \frac{1}{(K-m)} \sum_{t=m}^{N} \tilde{\mathbf{y}}(t)\tilde{\mathbf{y}}(t)^H, \tag{24}$$

where $\tilde{\mathbf{y}}(t) = [\mathbf{y}(t), \ldots, \mathbf{y}(t-m)]^T$. The MUSIC estimator from Section II which uses $\hat{\mathbf{R}}$ for ToF estimation is known as the forward approach. This is because the matrix $\hat{\mathbf{R}}$ appears in least-squares estimation of the coefficients $\{a_k\}$ of the $(m+1)$th-order forward linear predictor of $\mathbf{y}^*(t+1)$ [27]

$$\mathbf{y}^*(t+1) = a_0\mathbf{y}^*(t) + \ldots + a_m\mathbf{y}^*(t-m). \tag{25}$$

The estimation accuracy can be enhanced by using the following modification on the sample covariance matrix $\hat{\mathbf{R}}$

$$\tilde{\mathbf{R}} = \frac{1}{2}(\hat{\mathbf{R}} + \mathbf{J}_{m+1}\hat{\mathbf{R}}^*\mathbf{J}_{m+1}), \tag{26}$$

where

$$\mathbf{J}_{m+1} = \begin{bmatrix} 0 & & 1 \\ & \ddots & \\ 1 & & 0 \end{bmatrix}, \tag{27}$$

is the exchange matrix. The second term in (26) appears in the least-squares estimate of the coefficients of an $(m+1)$th-order backward predictor [27]. This property of $\mathbf{J}_{m+1}\hat{\mathbf{R}}^*\mathbf{J}_{m+1}$ suggests the name forward-backward averaging approach for methods that estimate signal parameters using $\tilde{\mathbf{R}}$. This forward-backward averaging also improves the condition number of $\hat{\mathbf{R}}$ which, in turn, improves the range estimation accuracy in multipath environments.

B. BANDWIDTH EXTRAPOLATION

The range estimation accuracy of the MUSIC or sparsity-aware estimators is limited by the available Bluetooth bandwidth because the ToF resolution is inversely proportional to the bandwidth. By using bandwidth extrapolation (BWE), the CFR can be extended virtually to achieve better resolution [28]. The linear-prediction signal model is one of the most practical models for the measurement data which assumes that the sum of uniformly-spaced signal samples multiplied by a set of complex weights will predict the next sample. These coefficients can span in the forward direction to continue predicting the signal samples outside the available bandwidth resulting in forward extrapolation. The complex conjugates of these prediction coefficients are used to predict the signal samples in the backward direction.

The prediction coefficients are estimated by applying least-squares methods to minimize the squared error between the estimated and actual measurement data, also known as forward-backward prediction error minimization. The extrapolation methods vary depending on how these prediction coefficients are estimated. Here, we apply Burg's method [29] to estimate the prediction coefficients which puts a constraint based on an auto-regressive all-pole model (the so-called Levison recursion) on the coefficients so that the extrapolated data do not increase in amplitude exponentially. Let the mth-order complex forward prediction coefficients estimated using Burg's algorithm be $a(n), n = 0, \ldots, m$. The forward and backward prediction lengths are K_f and K_b, respectively. We predict the measurement data sample-by-sample in the forward direction using

$$y_f(k) = -\sum_{t=1}^{m} y(k-t)a(t), \quad k = K, \ldots, K+K_f-1, \tag{28}$$

and in the backward direction using

$$y_b(k) = \sum_{t=1}^{m} y(k+t)a^*(t), \quad k = -1, \ldots, -K_b, \tag{29}$$

where, $y_f(k), k = K, \ldots, K+K_f-1$ is the forward predicted and $y_b(k), k = -1, \ldots, -K_b$ is the backward predicted CFR.

C. MULTI-ANTENNA COMBINING

When multiple antennas are available at the Initiator or Reflector or both sides, different antenna paths can be combined to provide spatial diversity that helps in mitigating multipath effects. We present two methods to utilize multi-antenna measurements; namely, Individual Antenna Processing (IAP) and Summed Antenna Processing (SAP) [6].

1) INDIVIDUAL ANTENNA PROCESSING (IAP)

In IAP, all antenna paths are processed separately by applying the range estimator to each path's CFR. Then, the minimum of all range estimates is selected as the final LOS distance. Let the estimated distance from the lth antenna path be $\hat{d}^{(l)}$. Using IAP, the final estimated distance is

$$\hat{d} = \min_{l=1,\ldots,L} \hat{d}^{(l)}. \tag{30}$$

By taking the minimum of all distance estimates from multiple antennas, the distance over-estimation error due to multipath is reduced. IAP can be applied to both the MUSIC and sparsity-aware estimators.

2) SUMMED ANTENNA PROCESSING (SAP)

The covariance matrices from individual antenna paths are summed in SAP for MUSIC distance estimation to achieve higher accuracy. In addition, by summing the covariance matrices, the EVD only needs to be computed once, thus reducing computational complexity. If $\hat{\mathbf{R}}^{(l)}$ is the covariance matrix for antenna path l, the summed covariance matrix for SAP is given by

$$\hat{\mathbf{R}} = \sum_{l=1,\ldots,L} \hat{\mathbf{R}}^{(l)}. \tag{31}$$

VI. REDUCED COMPLEXITY RANGE ESTIMATOR

The MUSIC range estimator computational complexity is dominated by the EVD and pseudospectrum computation in (19). In this section, we present two methods to reduce the MUSIC algorithm complexity; namely, using the signal subspace (as opposed to the noise subspace) to speed up the

MUSIC pseudospectrum computation and using the Lanczos algorithm [30] to reduce EVD complexity. Then, we compare the MUSIC and sparse OMP estimators' complexities in terms of the number of complex multiplications.

A. SIGNAL SUBSPACE BASED PSEUDOSPECTRUM

The MUSIC pseudospectrum in (19) is based on the noise eigenvectors. For signal subspace dimension q, the noise eigenvectors matrix dimension is $(m+1)\times(m-q+1)$. Under a fixed number of sources assumption, q remains constant. However, with an increasing measurement data size, the number of columns of $\mathbf{U}_n$ increases linearly. To reduce the computational cost of the MUSIC pseudospectrum computation, we use the signal subspace instead of the noise subspace as follows [31],

$$J(\tau)=\frac{1}{(m+1)-\left\|\mathbf{U}_s^H\Phi^m(\tau)\right\|_2^2}. \tag{32}$$

Proof: See Appendix A.

B. LANCZOS ALGORITHM FOR EIGENVECTOR APPROXIMATION

After separating the noise and signal eigenvectors of the sample covariance matrix using EVD in (18), which requires at least $O(M^3)$ flops for an $M\times M$ matrix, we are only interested in either the signal or the noise eigenvectors for pseudospectrum computation. To reduce the computational load of MUSIC, several iterative approaches have been proposed in the literature to estimate only the "most useful"[1] eigenvectors instead of computing all of them [32]. We apply the well-known Lanczos algorithm here to estimate the signal eigenvectors [30]. To approximate the signal eigenvectors of the Hermitian covariance matrix $\hat{\mathbf{R}}$, we first generate the orthonormal basis of the Krylov subspace of $\hat{\mathbf{R}}$ [33]. To do this, $\hat{\mathbf{R}}$ is first reduced to a symmetric tridiagonal form using the Lanczos algorithm. After the kth iteration of the Lanczos algorithm, we will have k basis vectors for the Krylov subspace which we denote by $[q_1,\ldots,q_k]$ (also called the Lanczos vectors). Then, we can write the tridiagonal matrix $\mathbf{T}_k$ as

$$\mathbf{T}_k=[q_1,\ldots,q_k]^T\hat{\mathbf{R}}[q_1,\ldots,q_k]=\mathbf{Q}_k^T\hat{\mathbf{R}}\mathbf{Q}_k. \tag{33}$$

After performing the above tri-diagonalization operation, we approximate the q signal eigenvalues using the Rayleigh-Ritz method [34] which approximates the eigenvalues of $\hat{\mathbf{R}}$ by the eigenvalues of $\mathbf{T}_k$, which are called Ritz values. If $\mathbf{T}_k=\mathbf{V}\Lambda\mathbf{V}^T$ is the eigen-decomposition of $\mathbf{T}_k$, the corresponding eigenvector approximations are the columns of $\mathbf{Q}_k\mathbf{V}$, which are called the Ritz vectors.

C. COMPLEXITY ANALYSIS

In this subsection, we compare the computational complexity of MUSIC (using either EVD or Lanczos algorithms) and sparse OMP estimators in terms of the number of complex multiplications. We assume that the number of search points used by MUSIC and sparse OMP are J_M and J_S, respectively. Table 4 shows the number of complex multiplications for the MUSIC and sparse range estimators. For the MUSIC estimator, the EVD and Lanczos algorithms are applied to compute the signal and noise subspaces for multi-antenna processing methods SAP and IAP. For fixed search grids of lengths J_M and J_S for the MUSIC and sparse estimators, respectively, a fixed number of sources q, and $K\approx\frac{m}{2}$, MUSIC using noise eigenvectors and EVD has computational complexity $\mathcal{O}(m^3)$, whereas MUSIC using signal subspace with Lanczos algorithm and sparse OMP estimators have computational complexities $\mathcal{O}(m^2)$ and $\mathcal{O}(m)$, respectively. Though the computational complexities of MUSIC using noise and signal subspace with EVD are $\mathcal{O}(m^3)$, using the signal subspace requires less complex multiplications due to no m^2 terms, as seen in Table 4. Figure 1 depicts the variation of computational complexity with data size. With forward and backward bandwidth extrapolation length of 30, the number of Bluetooth channels will increase from $K=80$ to 140. As expected, the computational complexity of the SAP estimators is lower than that of the IAP estimators since it is multiplied by the number of antennas in IAP. Among the IAP estimators, sparse OMP has the lowest computational complexity. The complexity reduction methods based on the signal subspace and Lanczos methods are shown to reduce the number of complex multiplications for the MUSIC estimators significantly with increasing K.

TABLE 4. Computational complexity of MUSIC and sparse OMP range estimators.

Multi-antenna processing	Estimator	No. of Multiplications
Summed Antenna Processing (SAP)	MUSIC (noise + EVD)	$m^2(K-m)+\frac{2}{3}m^3+2m(m-q+\frac{1}{2}J_M)J_M$
	MUSIC (signal + EVD)	$m^2(K-m)+\frac{2}{3}m^3+2m(q+\frac{1}{2}J_M)J_M$
	MUSIC (signal + Lan.)	$m^2(K-m)+3qm^2+2m(q+\frac{1}{2}J_M)J_M$
	Sparse OMP	N/A
Individual Antenna Processing (IAP)	MUSIC (noise + EVD)	$L\{m^2(K-m)+\frac{2}{3}m^3+2m(m-q+\frac{1}{2}J_M)J_M\}$
	MUSIC (signal + EVD)	$L\{m^2(K-m)+\frac{2}{3}m^3+2m(q+\frac{1}{2}J_M)J_M\}$
	MUSIC (signal + Lan.)	$L\{m^2(K-m)+3qm^2+2m(q+\frac{1}{2}J_M)J_M\}$
	Sparse OMP	$L\{\frac{KJ_Sq^2(q-1)}{2}+2q^3(K+q+1)\}$

VII. DATA COLLECTION

In this section, we describe our Bluetooth data collection campaign. For multipath multi-antenna scenarios, measure-

[1] "Most useful" eigenvectors refer to either the signal or noise eigenvectors since to compute the MUSIC pseudospectrum, either the signal or the noise eigenvectors are needed and the remaining eigenvectors can be ignored.

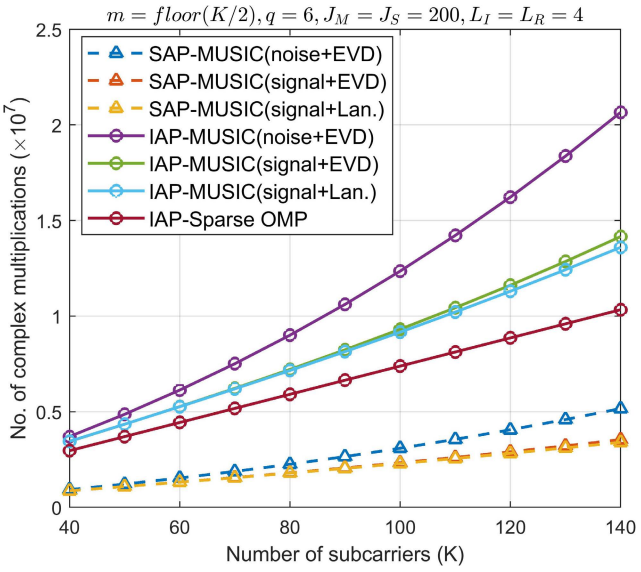

FIGURE 1. Number of complex multiplications as a function of data size K for SAP and IAP ranging estimators.

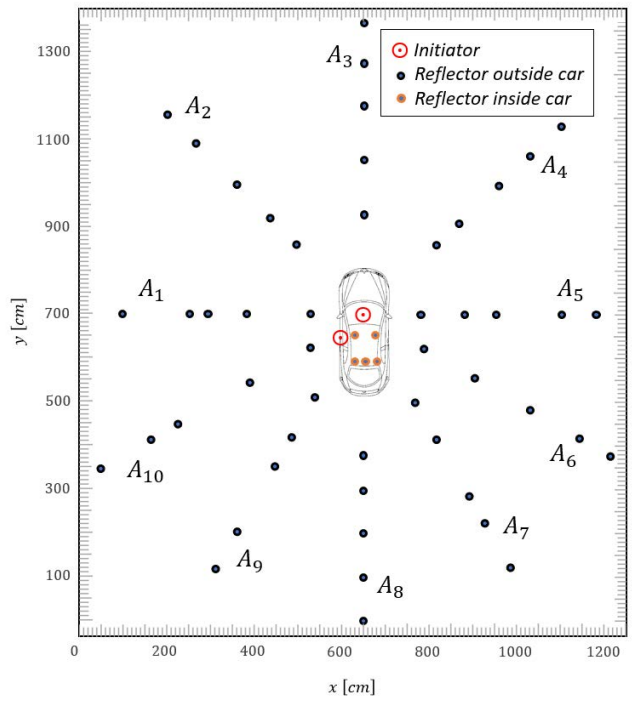

FIGURE 2. Locations of Initiator and Reflector in parking lot data collection campaign for LOS and NLOS multipath scenarios and antenna configurations 4 × 1, 1 × 4 and 2 × 2.

ments were taken in the parking lot where the Reflector was placed in varying positions inside and outside the car and the Initiator was fixed at two locations: outside the car on the door handle and inside the car on the rear-view mirror. The distance between the Initiator and Reflector is varied from 123cm to 700cm outside the car and from 84cm to 136cm inside the car. Figure 2 shows the measurements

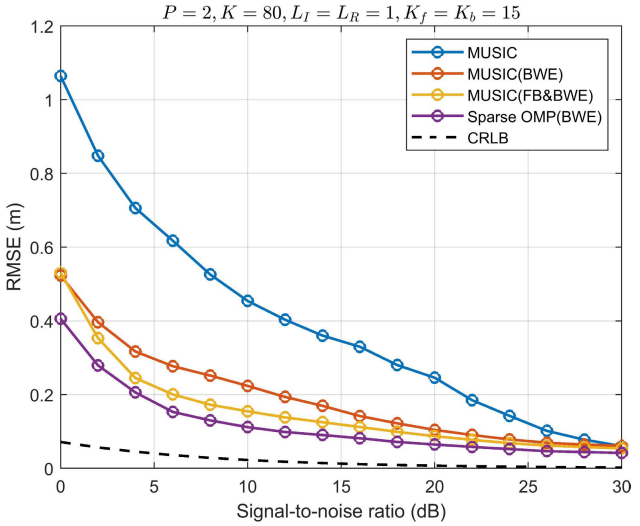

FIGURE 3. RMSE of enhanced super-resolution MUSIC and sparse OMP range estimators for $K = 80$ and $\Delta_f = 1$MHz.

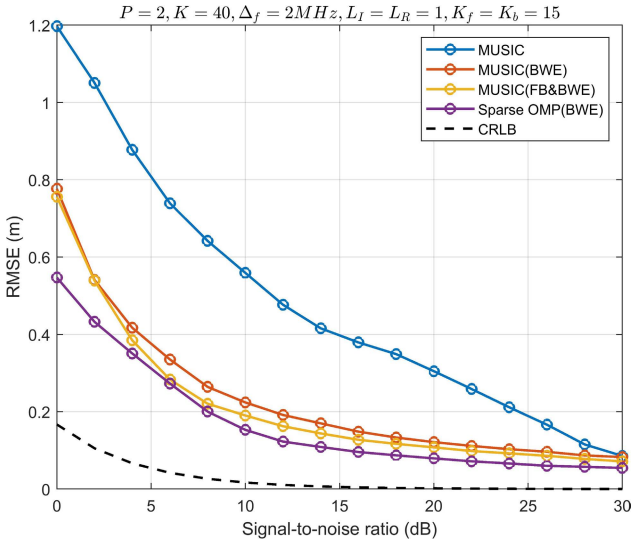

FIGURE 4. RMSE of enhanced super-resolution MUSIC and sparse OMP range estimators for $K = 40$ and $\Delta_f = 2$MHz.

collected with the fixed Initiator locations. The Reflector location is varied around the car in ten different directions of arrival. A_i denotes the dataset for the ith direction of arrival. For each location of the Reflector shown in Figure 2, 40 channel measurements were taken in the parking lot. For each direction of arrival, 5 Reflector locations were used. For each trial, both LOS and NLOS data were taken for antenna configurations 4 × 1, 1 × 4 and 2 × 2 (no. of antennas at Initiator × no. of antennas at Reflector). The measurements are defined as NLOS if there was user blockage, car blockage, or car seat blockage inside the car. The distances between the Initiator and Reflector inside the car were 84, 91, 130, 135, and 136cm. The Initiator to Reflector distances of the parking lot data collection campaign for each direction and Reflector location are summarized in Table 5.

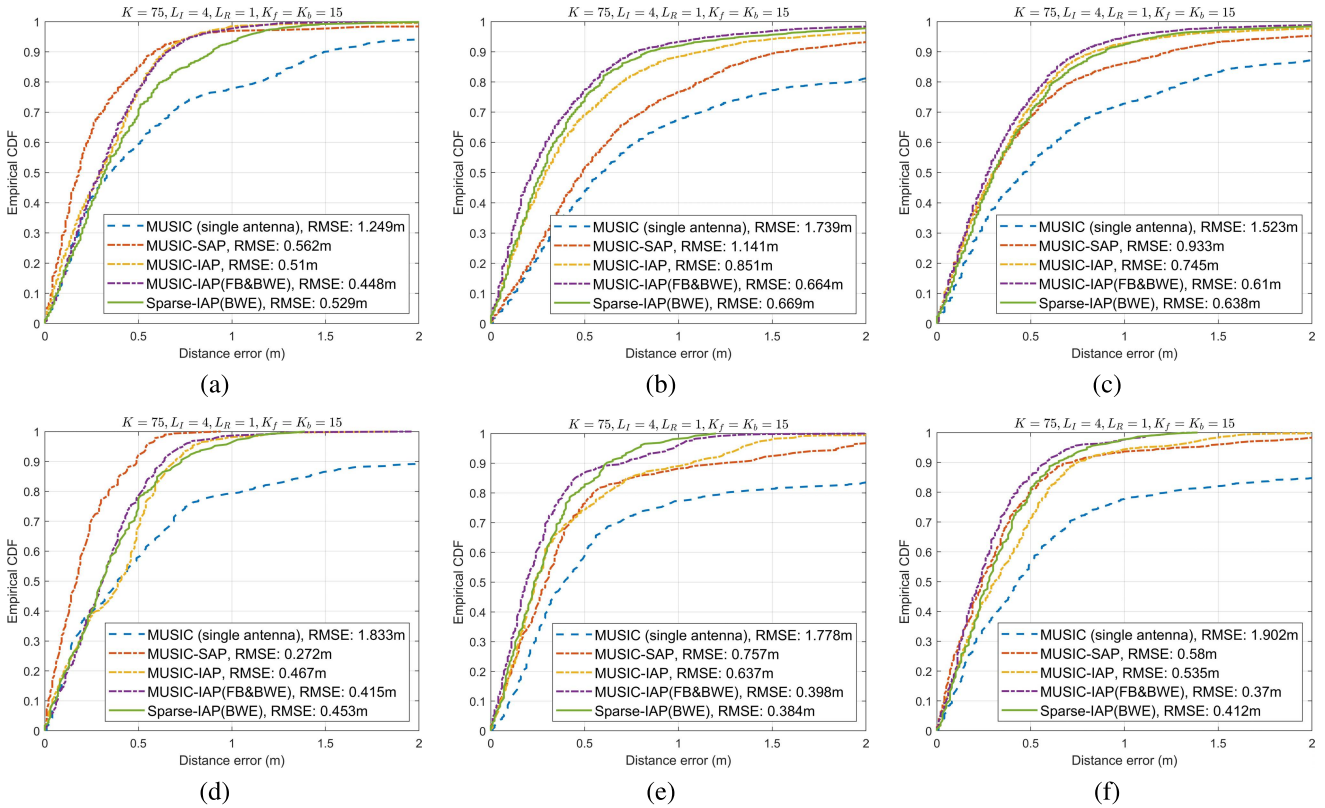

FIGURE 5. ECDF and RMSE performance of the investigated range estimators for collected bluetooth data when the initiator is inside the car and the Reflector is outside the car: (a) LOS, all distances, (b) NLOS, all distances, (c) LOS & NLOS, all distances, (d) LOS, distances ≤ 3m, (e) NLOS, distances ≤ 3m, (f) LOS & NLOS, distances ≤ 3m.

TABLE 5. Distances for collected bluetooth data sets $A_{i,i=1,2,3,4}$ and locations $L_{j,j=1,2,3,4,5}$.

Dataset	L_1 (cm)	L_2 (cm)	L_3 (cm)	L_4 (cm)	L_5 (cm)
A_1	123	272	357	401	556
A_2	145	306	493	562	700
A_3	229	335	414	585	682
A_4	310	400	500	600	700
A_5	132	231	305	452	531
A_6	168	307	447	578	660
A_7	244	342	493	565	681
A_8	218	309	410	543	638
A_9	239	352	479	574	667
A_{10}	230	305	428	526	623

VIII. NUMERICAL RESULTS

In this section, we present numerical results that quantify the performance of our investigated range estimators for simulated and collected Bluetooth data. First, we describe the simulation setup and system parameters for multi-antenna Bluetooth 5.1 transceivers. We compute the Cramer-Rao Lower Bound (CRLB) [35] for the two-way multipath channel and compare the performance of the enhanced ranging algorithms relative to the plain MUSIC algorithm and the CRLB. Next, we present the performance of ranging algorithms in practical scenarios with the collected Bluetooth data using the setups described in Section VII. The CRLB derivation is provided in Appendix B.

In the simulation setup, we assume a Bluetooth bandwidth of 80MHz with 80 hopping frequencies (channels) in the 2.4GHz band with frequency spacing of 1MHz. We consider a two-path channel where the distances travelled by the MPCs are set to $\{2, 4\}$ m with corresponding average powers of $\{0, -3\}$ dB. We compute the root mean square error (RMSE)[2] of the range estimators using 10, 000 Monte Carlo trials and compare it to the CRLB in (39).

Figure 3 depicts the RMSE performance of the enhanced MUSIC and sparse OMP estimators compared with the plain MUSIC estimator as a function of the signal-to-noise ratio (SNR). The bandwidth extrapolation parameter is $K_f = K_b = 15$. The enhancements of forward-backward averaging and bandwidth extrapolation are denoted by FB and BWE, respectively, and it is evident that they significantly improve the performance of MUSIC at medium and low SNR. For example, at SNR of 5 dB, MUSIC(BWE), MUSIC(FB&BWE) and Sparse OMP(BWE) reduce RMSE from 67cm to 32cm, 22cm, and 18cm, respectively. The variant MUSIC(FB&BWE) performs the best among the MUSIC estimators and Sparse OMP(BWE) performs the best overall in this single-antenna two-path channel scenario.

[2]For LOS distance x_i and estimated distance $\hat{x}_i$ at ith trial, the RMSE is calculated as $\sqrt{\frac{\sum_{i=1}^{N}(x_i-\hat{x}_i)^2}{N}}$ for N number of trials.

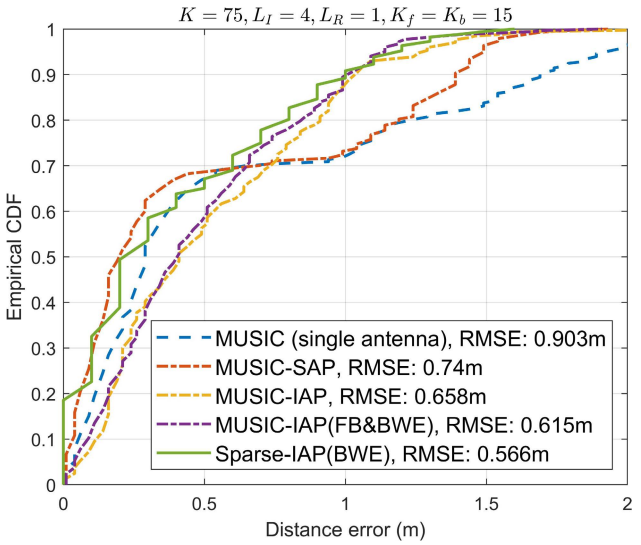

FIGURE 6. ECDF and RMSE performances of the investigated range estimators when the Initiator is on the car door handle, the Reflector is outside the car, and LOS distances ≤ 3m.

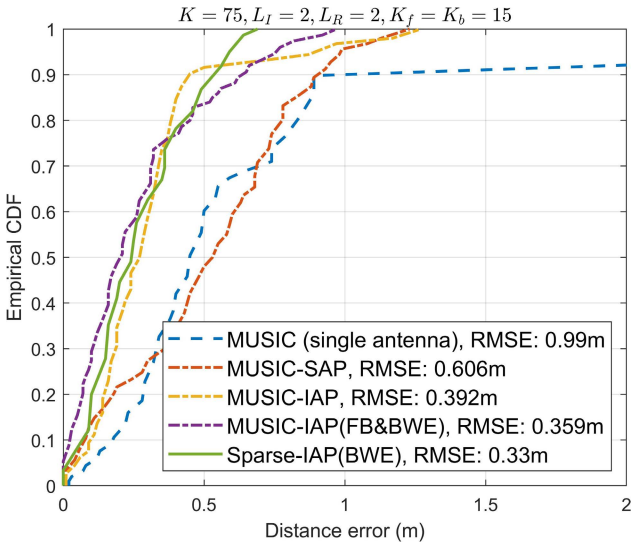

FIGURE 7. ECDF and RMSE performance of the investigated range estimators when the Initiator and Reflector are both inside the car.

The Bluetooth Low Energy (BLE) standard uses the same total bandwidth of 80 MHs as classical Bluetooth. However, the number of frequencies is halved to $K = 40$ and their spacing is doubled to $\Delta_f = 2$MHz. It is clear from Figure 4 that the ranging RMSE is increased in BLE due to the reduced frequency resolution of the CFR.

For our collected Bluetooth data, the ECDF performances in multipath environments LOS, NLOS and both LOS-NLOS where the Initiator is on the rear-view mirror of the car and the Reflector is outside the car are shown in Figure 5. The best performing estimators, namely, MUSIC-SAP, MUSIC-IAP, MUSIC-IAP with FB and BWE enhancements (MUSIC-IAP(FB&BWE)) and sparse OMP IAP with BWE enhancement (Sparse-IAP(BWE)) are compared with the plain single-antenna MUSIC estimator. In almost all of these scenarios, the MUSIC-IAP(FB&BWE) and Sparse-IAP(BWE) are comparable in terms of the 90th percentile error[3] and RMSE while outperforming all other estimators. MUSIC-SAP performs the best in terms of the 90th percentile error when the LOS is present and in terms of RMSE (27cm, which is 85% better than the single-antenna plain MUSIC) when the LOS distances are smaller than or equal to 3m. The sparse OMP estimator performance is very close to the MUSIC-IAP(FB&BWE) in all of these scenarios.

However, as shown in Section VI, the sparse OMP estimator has much lower complexity than the MUSIC estimator. Figure 6 depicts the performances of the range estimators when the Initiator is on the car door handle, the Reflector is outside the car, and the LOS distances are smaller than or equal to 3m. The sparse OMP estimator outperforms the other estimators in this scenario both in terms of the 90th percentile error and its RMSE of 56.6cm, which represents a 38% performance improvement over the RMSE of the single-antenna plain MUSIC estimator.

Finally, Figure 7 shows the performances of the investigated range estimators when both the Initiator and Reflector are inside the car for the 2×2 antenna configuration. In this scenario, the sparse OMP estimator achieves the best RMSE performance of 33cm, which represents a 67% performance improvement over the single-antenna plain MUSIC estimator.

IX. CONCLUSION

In this paper, we investigated enhanced super-resolution MUSIC and sparsity-aware OMP range estimators for two-way Bluetooth signalling. We presented the results of our Bluetooth real-world data collection campaign in different multipath scenarios with three different Initiator-Reflector pair locations and antenna configurations. In addition, we analyzed complexity reduction methods for the MUSIC estimator using the Lanczos algorithm and by utilizing the signal subspace instead of the noise subspace for MUSIC pseudospectrum computation. Furthermore, we demonstrated the performance gains of forward-backward sample covariance matrix averaging for MUSIC and bandwidth extrapolation for both MUSIC and OMP estimators. For multi-antenna processing, we compared two methods, namely, Individual Antenna Processing (IAP) and Summed Antenna Processing (SAP), to combine multiple antenna measurements.

To compare the performances of our investigated range estimators, we evaluated their ECDF and RMSE both for simulated and collected Bluetooth data. Our numerical results showed significant performance improvement from the enhancements on MUSIC and sparse OMP estimators in all multipath scenarios. Our proposed enhanced range estimators improved the ranging accuracy by 58% for our collected Bluetooth data for a range up to 7m for both LOS

[3]The 90th percentile error is defined to be the absolute error at which or below which 90% of the absolute errors occur.

and NLOS multipath scenarios. For example, in the scenario with all LOS distances and both LOS and NLOS environments, MUSIC-SAP, MUSIC-IAP, MUSIC-IAP(FB&BWE) and Sparse-IAP(BWE) reduce the RMSE from 1.53m (for the single-antenna case without enhancements) to 93cm, 75cm, 61cm, and 64cm, respectively. Even though MUSIC-IAP achieves higher performance than MUSIC-SAP in terms of RMSE and 90th percentile error in almost all scenarios, it has higher computational complexity. For a data size of $K = 80$, MUSIC-SAP (with 0.22×10^7 complex multiplications) is around 4 times faster compared to MUSIC-IAP (0.9×10^7 complex multiplications). The sparse OMP (with 0.63×10^7 complex multiplications for data size $K = 80$) has the lowest complexity of all the enhanced IAP estimators (1.43 times faster than MUSIC-IAP) and performs very close to the MUSIC IAP with FB and BWE enhancements. With increasing data size, sparse OMP becomes even faster than MUSIC-IAP (2.2 times faster for data size $K = 140$). Therefore, enhanced sparse OMP is clearly the best candidate for range estimation among all IAP estimators investigated in this paper because of its low RMSE, 90th percentile error, and reduced complexity compared to the enhanced MUSIC estimators.

In conclusion, key advantages of our investigated ranging solutions for IoT networks using Bluetooth signals include decimeter-level high accuracy, low power consumption, low deployment cost due to the use of existing ubiquitous Bluetooth signals, applicability to both indoor and outdoor scenarios within Bluetooth range, and implementation using simple firmware upgrades without the need for expensive dedicated hardware as in Ultra-Wideband (UWB) based ranging. Disadvantages are the limited Bluetooth bandwidth and limited range which we will address in our future work by investigating ranging using WiFi signals and possibly fusing them with Bluetooth signals across the 2.4 and 5 GHz unlicensed frequency bands for better accuracy in an NLOS multipath environment.

APPENDIX A
DERIVATION OF SIGNAL SUBSPACE BASED MUSIC PSEUDO-SPECTRUM

We want to prove the following equation

$$J(\tau) = \frac{1}{\left\|\mathbf{U}_n^H \Phi^m(\tau)\right\|_2^2} = \frac{1}{(m+1) - \left\|\mathbf{U}_s^H \Phi^m(\tau)\right\|_2^2}. \quad (34)$$

For the signal and noise eigenvector matrices denoted by $\mathbf{U}_s$ and $\mathbf{U}_n$, respectively, we can write

$$\sum_{i=1}^{q} \left\|\Phi^H(\tau)\mathbf{u}_i\right\|_2^2 + \sum_{i=q+1}^{m+1} \left\|\Phi^H(\tau)\mathbf{u}_i\right\|_2^2 = \sum_{i=1}^{m+1} \left\|\Phi^H(\tau)\mathbf{u}_i\right\|_2^2, \quad (35)$$

where $\mathbf{u}_n$ is the nth column of eigenvector matrix $\mathbf{U} = [\mathbf{U}_s \ \mathbf{U}_n]$. We write the summation in terms of vectors as

$$\sum_{i=1}^{m+1} \left\|\Phi^H(\tau)\mathbf{u}_i\right\|_2^2 = \Phi^H(\tau)\mathbf{U}\mathbf{U}^H\Phi(\tau). \quad (36)$$

For orthonormal eigenvectors, $\mathbf{U}\mathbf{U}^H = \mathbf{I}$. Hence,

$$\Phi^H(\tau)\mathbf{U}\mathbf{U}^H\Phi(\tau) = \Phi^H(\tau)\Phi(\tau) = m+1, \quad (37)$$

since $\Phi(\tau) = [1, e^{-j2\pi\Delta_f\tau}, e^{-j2\pi 2\Delta_f\tau}, \ldots, e^{-j2\pi m\Delta_f\tau}]$. Finally, we equate the denominators of the two pseudospectrums to get

$$\sum_{i=q+1}^{m+1} \left\|\Phi^H(\tau)\mathbf{u}_i\right\|_2^2 = (m+1) - \sum_{i=1}^{q} \left\|\Phi^H(\tau)\mathbf{u}_i\right\|_2^2. \quad (38)$$

APPENDIX B
DERIVATION OF ToF CRAMER-RAO LOWER BOUND FOR TWO-PATH CHANNEL

The CRLB for the system model described in (2) sets a lower bound on the variance of any unbiased estimator for the ToF of the LOS path. This CRLB was derived and further simplified under the Wide Sense Stationary uncorrelated Scattering (WSSUS) channels assumption in [36]. The final CRLB expression for MPC delay τ_k was shown to be given by

$$\text{CRLB}(\tau_k) = \frac{1}{2(K-m)\cdot SNR_k} b^{-1}(\tau_k), \quad (39)$$

where SNR_k is the SNR of the kth MPC, $b(\tau_k) = \mathbf{d}^H(\tau_k)(\mathbf{I} - \mathbf{P_H})\mathbf{d}(\tau_k)$, $\mathbf{P_H} = \mathbf{H}(\mathbf{H}^H\mathbf{H})^{-1}\mathbf{H}^H$ is the projection matrix on the column space of $\mathbf{H}$, where $\mathbf{H}$ is the array manifold matrix in (7), and $\mathbf{d}(\tau_k)$ is the kth column of $\mathbf{D}$ where

$$\mathbf{D} = [\frac{\partial \boldsymbol{\gamma}(\tau_1)}{\partial \tau_1}, \ldots, \frac{\partial \boldsymbol{\gamma}(\tau_p)}{\partial \tau_p}], \quad (40)$$

is the matrix of derivatives of the steering vectors with respect to the delays. As seen from the CRLB(τ_k) expression in (39), the CRLB is inversely proportional to the SNR of the kth MPC, denoted by SNR_k, and to the number of hopping Bluetooth frequencies in excess of the smoothing length, give by $K-m$. In addition, the CRLB is also inversely proportional to the scalar positive quantity $b(\tau_k)$, which has a quadratic form that is equal to the magnitude square of the error vector when projecting $d(\tau_k)$ on the column space of $\mathbf{H}$.

To gain more insights, we will derive a simplified closed-form CRLB expression for the special case of a two-path CIR, where $P = 2$ and $\mathbf{H} = [\boldsymbol{\gamma}(\tau_1), \boldsymbol{\gamma}(\tau_2)]$. Since $\mathbf{P_H}$ is a projection matrix, we can write (using Pythagoras Theorem)

$$\begin{aligned} b(\tau_k) &= \|(\mathbf{I} - \mathbf{P_H})\mathbf{d}(\tau_k)\|_2^2 \\ &= \|\mathbf{d}(\tau_k)\|_2^2 - \|\mathbf{P_H}\mathbf{d}(\tau_k)\|_2^2. \end{aligned} \quad (41)$$

For the first CIR path with ToF τ_1, we have

$$\mathbf{d}(\tau_1) = -j2\pi\Delta_f[0, e^{-j2\pi\Delta_f\tau_1}, \ldots, (K-1)e^{-j2\pi(K-1)\Delta_f\tau_1}]^T. \quad (42)$$

Therefore, the quantity $\|\mathbf{d}(\tau_1)\|_2^2 = \frac{2\pi^2\Delta_f^2 K(K-1)(2K-1)}{3}$ does not depend on the ToFs of any of the CIR paths. The second term in (41) can be expanded as $\|\mathbf{P_H}\mathbf{d}(\tau_1)\|_2^2 = \left\|\mathbf{H}(\mathbf{H}^H\mathbf{H})^{-1}\mathbf{H}^H\mathbf{d}(\tau_1)\right\|_2^2$ where the psuedo inverse matrix $\mathbf{H}(\mathbf{H}^H\mathbf{H})^{-1}$ and the column vector $\mathbf{H}^H\mathbf{d}(\tau_1)$ are given by

$$\begin{aligned}&\mathbf{H}(\mathbf{H}^H\mathbf{H})^{-1}\\ &= \begin{bmatrix}\boldsymbol{\gamma}(\tau_1) & \boldsymbol{\gamma}(\tau_2)\end{bmatrix}\left(\begin{bmatrix}\boldsymbol{\gamma}^H(\tau_1)\\ \boldsymbol{\gamma}^H(\tau_2)\end{bmatrix}\begin{bmatrix}\boldsymbol{\gamma}(\tau_1) & \boldsymbol{\gamma}(\tau_2)\end{bmatrix}\right)^{-1}\\ &= \frac{\begin{bmatrix}K\boldsymbol{\gamma}(\tau_1) - \boldsymbol{\gamma}(\tau_2)\boldsymbol{\gamma}^H(\tau_2)\boldsymbol{\gamma}(\tau_1)\\ K\boldsymbol{\gamma}(\tau_2) - \boldsymbol{\gamma}(\tau_1)\boldsymbol{\gamma}^H(\tau_1)\boldsymbol{\gamma}(\tau_2)\end{bmatrix}^T}{K^2 - \left\|\boldsymbol{\gamma}^H(\tau_2)\boldsymbol{\gamma}(\tau_1)\right\|_2^2},\end{aligned} \tag{43}$$

$$\begin{aligned}&\mathbf{H}^H\mathbf{d}(\tau_1)\\ &= -j2\pi\Delta_f\begin{bmatrix}\boldsymbol{\gamma}^H(\tau_1)\\ \boldsymbol{\gamma}^H(\tau_2)\end{bmatrix}\begin{bmatrix}0\\ e^{-j2\pi\Delta_f\tau_1}\\ \vdots\\ (K-1)e^{-j2\pi(K-1)\Delta_f\tau_1}\end{bmatrix},\end{aligned} \tag{44}$$

where $\delta_\tau = \tau_2 - \tau_1$ is the ToF difference between the two CIR paths. For Bluetooth, $K = 80$, $\Delta_f = 1$MHz, and the distance separation between the two paths can be assumed less than 15 meters. Hence, we can use the approximations $\sin 2\pi\Delta_f\delta_\tau \approx 2\pi\Delta_f\delta_\tau$, $\cos 2\pi\Delta_f\delta_\tau \approx 1$, and $e^{j2\pi(K-1)\Delta_f\delta_\tau} \approx e^{j2\pi K\Delta_f\delta_\tau}$. Using these approximations, $\left\|\boldsymbol{\gamma}^H(\tau_2)\boldsymbol{\gamma}(\tau_1)\right\|_2^2$ can be written as K sinc $(K\Delta_f\delta_\tau)$.[4] Hence, the expression of $\|\mathbf{P_H}\mathbf{d}(\tau_1)\|_2^2$ simplifies to

$$\left\|\mathbf{H}(\mathbf{H}^H\mathbf{H})^{-1}\mathbf{H}^H\mathbf{d}(\tau_1)\right\|_2^2 = \frac{K\zeta(\delta_\tau)}{\delta_\tau^2(1-\text{sinc}^2(K\Delta_f\delta_\tau))^2}, \tag{45}$$

where

$$\begin{aligned}&\zeta(\delta_\tau)\\ &= \left\|\text{sinc}(\frac{K\beta}{\pi})\,(\beta(K-1)-j) + je^{jK\beta}\right\|_2^2\\ &\quad\times\Bigg(1 + \left\|\frac{\beta(K-1) - j\text{sinc}(\frac{K\beta}{\pi})\left(\text{sinc}(\frac{K\beta}{\pi}) + e^{jK\beta}\right)}{\text{sinc}(\frac{K\beta}{\pi})\,(\beta(K-1)-j) + je^{jK\beta}}\right\|_2^2\\ &\quad- 2\Re\left[\frac{\beta(K-1) - j\text{sinc}(\frac{K\beta}{\pi})\left(\text{sinc}(\frac{K\beta}{\pi}) + e^{jK\beta}\right)}{(\beta(K-1)-j) + \frac{je^{jK\beta}}{\text{sinc}(\frac{K\beta}{\pi})}}\right]\Bigg),\end{aligned} \tag{46}$$

and $\beta = \pi\Delta_f\delta_\tau$. The sinc function $\text{sinc}(K\Delta_f\delta_\tau)$ equals zero at $\delta_\tau = \frac{n}{K\Delta_f}$, $n = 1, 2, \ldots$. At these values of ToF difference, we have

$$\|\mathbf{P_H}\mathbf{d}(\tau_1)\|_2^2 = \frac{K}{(\delta_\tau)^2} + \pi^2\Delta_f^2K(K-1)^2. \tag{47}$$

[4]The normalized sinc function is defined for $x \neq 0$ as sinc $(x) = \frac{\sin(\pi x)}{\pi x}$. The value at $x = 0$ is defined to be the limiting value $\lim_{x\to 0}$ sinc $(x) = 1$. At $x = \pm1, \pm2, \ldots$, sinc $(x) = 0$.

Since $\|\mathbf{P_H}\mathbf{d}(\tau_1)\|_2^2$ is inversely proportional to δ_τ^2 with a steady-state value of $\pi^2\Delta_f^2K(K-1)^2$, we can approximate (45) accurately as follows

$$\|\mathbf{P_H}\mathbf{d}(\tau_1)\|_2^2 \approx \pi^2K\alpha^2\text{sinc}^2(\alpha\delta_\tau) + \pi^2\Delta_f^2K(K-1)^2, \tag{48}$$

where $\alpha = \frac{\Delta_fK}{\sqrt{3}}$ was determined by ensuring that the initial and steady-state values of the approximated function in (48) match those of $\|\mathbf{P_H}\mathbf{d}(\tau_1)\|_2^2$ in (45). This approximated expression can be used in (41) to compute the following closed-form expression of $b(\tau_1)$

$$b(\tau_1) \approx \frac{\pi^2}{3}K^3\Delta_f^2(1 - \text{sinc}^2(\alpha\delta_\tau)), \tag{49}$$

where we assumed $K^3 \gg K$ to simplify the expression of $b(\tau_1)$. For $\delta_\tau \leq \frac{\sqrt{3}}{2K\Delta_f}$, we can accurately approximate $b(\tau_1)$ with a quadratic function as follows

$$b(\tau_1) \approx \frac{4}{9}\left(\pi^2 - 4\right)K^5\Delta_f^4\delta_\tau^2. \tag{50}$$

For $\delta_\tau \geq \frac{\sqrt{3}}{K\Delta_f}$, the sinc function variation in (49) is so small that we can approximate $b(\tau_1)$ by a constant equal to the steady-state value in (49) as follows

$$b(\tau_1) \approx K^3\Delta_f^2\frac{\pi^2}{3}. \tag{51}$$

Putting all the approximations of $b(\tau_1)$ together, we have

$$b(\tau_1) = \begin{cases}\frac{4}{9}\left(\pi^2-4\right)K^5\Delta_f^4\delta_\tau^2 & : \delta_\tau \leq \frac{\sqrt{3}}{2K\Delta_f}\\ \frac{\pi^2}{3}K^3\Delta_f^2(1-\text{sinc}^2(\alpha\delta_\tau)) & : \frac{\sqrt{3}}{2K\Delta_f} \leq \delta_\tau \leq \frac{\sqrt{3}}{K\Delta_f}\\ K^3\Delta_f^2\frac{\pi^2}{3} & : \frac{\sqrt{3}}{K\Delta_f} \leq \delta_\tau.\end{cases} \tag{52}$$

We can gain the following insights from the above expression of $b(\tau_1)$ and when it is substituted in the CRLB expression in (39), at a given SNR of the first path.

- For the two-path channel model, the CRLB on variance of ToF estimation of each path depends on the ToF difference between the two paths δ_τ, not the individual paths ToFs.
- As the two paths become closer, δ_τ decreases and CRLB increases proportional to $\frac{1}{\delta_\tau^2}$.
- The CRLB decreases inversely proportional to δ_τ^2 until $\delta_\tau = \frac{\sqrt{3}}{2K\Delta_f}$ which is equal to 11 nano-seconds (or equivalently two-path distance separation of 3.3 meters) for Bluetooth parameters of $K = 80$ and $\Delta_f = 1$MHz. For $\delta_\tau \geq \frac{\sqrt{3}}{2K\Delta_f}$, the CRLB exhibits small additional oscillations due to the sinc function, as shown in the inset of Figure 8 below.
- For a fixed path separation $\delta_\tau \leq \frac{\sqrt{3}}{2K\Delta_f}$, the CRLB is well approximated by

$$CRLB(\tau_1) \approx \frac{9}{8(\pi^2-4)(K-m)K^5\Delta_f^4SNR_1\delta\tau^2}, \tag{53}$$

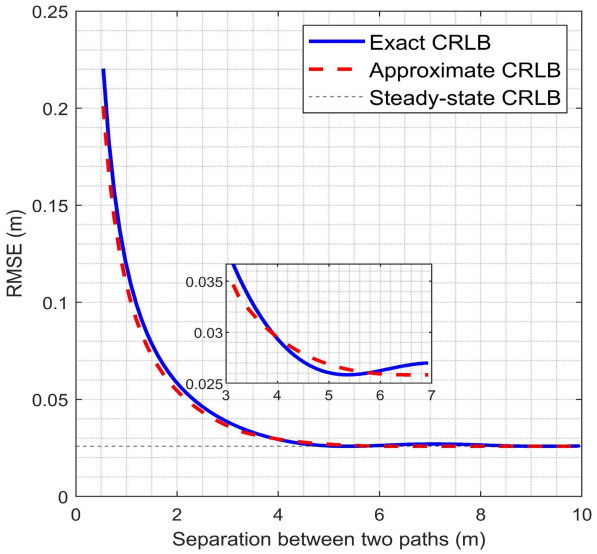

FIGURE 8. Exact and approximated CRLB plots of first path for a two-path channel with $K = 80$, $\Delta_f = 1$MHz, and $SNR_1 = 0$dB.

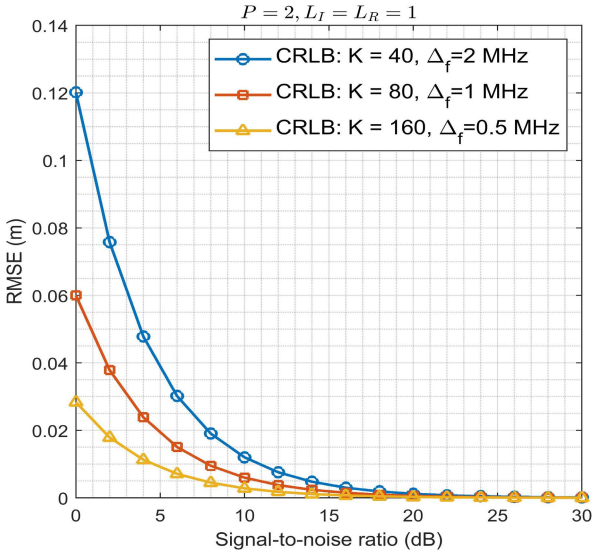

FIGURE 9. CRLB on ToF estimator RMSE of first path for a two-path channel with $K = 40, 80, 160$, $\Delta_f = 0.5, 1, 2$MHz, and path separation of 2m.

which decreases rapidly inversely proportional to K^6 and less rapidly inversely proportional to Δ_f^4. Hence, for a fixed δ_τ and fixed total bandwidth which is equal to $K\Delta_f$, doubling K and halving Δ_f will reduce the CRLB on the estimator variance by a factor of 4. On the other hand, halving K and doubling Δ_f (as in the BLE standard) will increase CRLB on estimator variance by a factor of 4 (or equivalently by a factor of 2 in estimator RMSE).

- For path separation $\delta_\tau \geq \frac{\sqrt{3}}{K\Delta_f}$ which is equal to 22 nano-seconds (or equivalently two-path distance separation of 6.6 meters), the CRLB approaches its steady state value $CRLB^{SS}$ given by

$$CRLB^{SS}(\tau_1) = \frac{3}{2\pi^2(K-m)K^3\Delta_f^2 SNR_1}, \qquad (54)$$

which is inversely proportional to the square of the frequency spacing Δ_f and the fourth power of the number of frequencies K. Hence, for a fixed total bandwidth, doubling K and halving Δ_f will reduce the steady-state CRLB on estimator variance by a factor of 4. On the other hand, halving K and doubling Δ_f will increase steady-state CRLB on estimator variance by a factor of 4 (or equivalently by a factor of 2 in estimator RMSE).

Figure 8 shows the excellent match between the exact and approximate CRLB for the two-path Bluetooth channel model. We assume a smoothing length $m = \frac{K}{2} = 40$ and $SNR_1 = 0$dB which, when substituted in (54), result in a steady-state CRLB of 0.09 nano-seconds or equivalently 2.58 cm as shown in Figure 8.

Finally, Figure 9 depicts the variation of the CRLB with the SNR of the first path for different choices of K and Δ_f while keeping the total bandwidth fixed at 80 MHz. As predicted accurately by our CRLB expression in (53), doubling the CFR frequency resolution by doubling K, reduces the CRLB on RMSE by a factor of 2.

ACKNOWLEDGMENT

The authors would like to thank Yaron Alpert, Matan Ben-Shachar, and Jianwei Zhou from Texas Instruments for many insightful discussions during this work.

Any opinions, findings, and conclusions or recommendations expressed in this material are those of the author(s) and do not necessarily reflect the views of the NSF.

REFERENCES

[1] C. Laoudias, A. Moreira, S. Kim, S. Lee, L. Wirola, and C. Fischione, "A survey of enabling technologies for network localization, tracking, and navigation," *IEEE Commun. Surveys Tuts.*, vol. 20, no. 4, pp. 3607–3644, 4th Quart., 2018.

[2] G. Han, J. Jiang, C. Zhang, T. Q. Duong, M. Guizani, and G. Karagiannidis, "A survey on mobile anchor node assisted localization in wireless sensor networks," *IEEE Commun. Surveys Tuts.*, vol. 18, no. 3, pp. 2220–2243, 3rd Quart., 2016.

[3] F. Zafari, A. Gkelias, and K. K. Leung, "A survey of indoor localization systems and technologies," *IEEE Commun. Surveys Tuts.*, vol. 21, no. 3, pp. 2568–2599, 3rd Quart., 2017.

[4] S. Kuutti, S. Fallah, K. Katsaros, M. Dianati, F. Mccullough, and A. Mouzakitis, "A survey of the state-of-the-art localization techniques and their potentials for autonomous vehicle applications," *IEEE Internet Things J.*, vol. 5, no. 2, pp. 829–846, Apr. 2018.

[5] A. Capponi, C. Fiandrino, B. Kantarci, L. Foschini, D. Kliazovich, and P. Bouvry, "A survey on mobile crowdsensing systems: Challenges, solutions, and opportunities," *IEEE Commun. Surveys Tuts.*, vol. 21, no. 3, pp. 2419–2465, 3rd Quart., 2019.

[6] P. Boer, J. Romme, J. Govers, and G. Dolmans, "Performance of high-accuracy phase-based ranging in multipath environments," in *Proc. 91st Veh. Technol. Conf.*, 2020, pp. 1–5.

[7] M. Pelka, C. Bollmeyer, and H. Hellbruck, "Accurate radio distance estimation by phase measurements with multiple frequencies," in *Proc. Int. Conf. Indoor Positioning Indoor Navigat. (IPIN)*, Oct. 2014, pp. 142–151.

[8] P. Zand, J. Romme, J. Govers, F. Pasveer, and G. Dolmans, "A high-accuracy phase-based ranging solution with Bluetooth low energy (BLE)," in *Proc. IEEE Wireless Commun. Netw. Conf. (WCNC)*, Dec. 2019, pp. 1–8.
[9] M. Gunia, A. Zinke, N. Joram, and F. Ellinger, "Setting up a phase-based positioning system using off-the-shelf components," in *Proc. 14th Workshop Positioning, Navigat. Commun. (WPNC)*, Oct. 2017, pp. 1–6.
[10] Y. Schroder, D. Reimers, and L. Wolf, "Accurate and precise distance estimation from phase-based ranging data," in *Proc. Int. Conf. Indoor Positioning Indoor Navigat. (IPIN)*, Sep. 2018, pp. 1–8.
[11] X. Li, E. Leitinger, M. Oskarsson, K. Åström, and F. Tufvesson, "Massive MIMO-based localization and mapping exploiting phase information of multipath components," *IEEE Trans. Wireless Commun.*, vol. 18, no. 9, pp. 4254–4267, Sep. 2019.
[12] X. Li and K. Pahlavan, "Super-resolution TOA estimation with diversity for indoor geolocation," *IEEE Trans. Wireless Commun.*, vol. 3, no. 1, pp. 224–234, Jan. 2004.
[13] M. C. Vanderveen, A.-J. van der Veen, and A. Paulraj, "Estimation of multipath parameters in wireless communications," *IEEE Trans. Signal Process.*, vol. 46, no. 3, pp. 682–690, Mar. 1998.
[14] Y. Hua, "Estimating two-dimensional frequencies by matrix enhancement and matrix pencil," *IEEE Trans. Signal Process.*, vol. 40, no. 9, pp. 2267–2280, Sep. 1992.
[15] W. Liao and A. Fannjiang, "MUSIC for single-snapshot spectral estimation: Stability and super-resolution," *Appl. Comput. Harmon. Anal.*, vol. 40, no. 1, pp. 33–67, 2016.
[16] Z. Yang, J. Li, P. Stoica, and L. Xie, "Sparse methods for direction-of-arrival estimation," in *Academic Press Library in Signal Processing*, vol. 7. Amsterdam, The Netherlands: Elsevier, 2018, pp. 509–581.
[17] Z. Yang and L. Xie, "On gridless sparse methods for line spectral estimation from complete and incomplete data," *IEEE Trans. Signal Process.*, vol. 63, no. 12, pp. 3139–3153, Jun. 2015.
[18] M. Wang H. Han D. Yang, J. Wang, and Y. Zhang, "Accuracy analysis of Bluetooth-low-energy ranging and positioning in NLOS environment," *Int. J. Image Data Fusion*, vol. 11, no. 4, pp. 356–374, 2020.
[19] D. Vasisht, S. Kumar, and D. Katabi, "Decimeter-level localization with a single WiFi access point," in *Proc. 13th Symp. Netw. Syst. Design Implement.*, 2016, pp. 165–178.
[20] A. Paulraj, V. U. Reddy, T. J. Shan, and T. Kailath, "Performance analysis of the MUSIC algorithm with spatial smoothing in the presence of coherent sources," in *Proc. IEEE Mil. Commun. Conf., Commun.-Comput.*, vol. 3, Dec. 1986, pp. 5–41.
[21] M. Wax and T. Kailath, "Detection of signals by information theoretic criteria," *IEEE Trans. Acoust., Speech, Signal Process.*, vol. ASSP-33, no. 2, pp. 387–392, Jun. 1985.
[22] D. L. Donoho and M. Elad, "Optimally sparse representation in general (nonorthogonal) dictionaries via ℓ_1 minimization," *Proc. Nat. Acad. Sci. USA*, vol. 100, no. 5, pp. 2197–2202, Mar. 2003.
[23] X. Tan, W. Roberts, J. Li, and P. Stoica, "Sparse learning via iterative minimization with application to MIMO radar imaging," *IEEE Trans. Signal Process.*, vol. 59, no. 3, pp. 1088–1101, Mar. 2011.
[24] T. Blumensath and M. E. Davies, "Iterative hard thresholding for compressed sensing," *Appl. Comput. Harmon. Anal.*, vol. 27, no. 3, pp. 265–274, Nov. 2009.
[25] D. L. Donoho, Y. Tsaig, I. Drori, and J.-L. Starck, "Sparse solution of underdetermined systems of linear equations by stagewise orthogonal matching pursuit," *IEEE Trans. Inf. Theory*. vol. 58, no. 2, pp. 1094–1121, Feb. 2006.
[26] J. A. Tropp and S. J. Wright, "Computational methods for sparse solution of linear inverse problems," *Proc. IEEE*, vol. 98, no. 6, pp. 948–958, Jun. 2010.
[27] P. Stoica and R. L. Moses, *Spectral Analysis of Signals*. Upper Saddle River, NJ, USA: Prentice-Hall, 2005.
[28] S. L. Borison, S. B. Bowling, and K. M. Cuomo, "Super-resolution methods for wideband radar," *Lincoln Lab. J.*, vol. 5, no. 3, pp. 441–461, 1992.
[29] J. P. Burg, "A new analysis technique for time series data," in *Proc. Adv. Study Inst. Signal Process.*, Enschede, Netherlands, 1968, pp. 1–5.
[30] G. H. Golub and C. E. Van Loan, *Matrix Computations*. Baltimore, MD, USA: The Johns Hopkins Univ. Press, 1989.
[31] J. T. Karhunen and J. Joutsensalo, "Sinusoidal frequency estimation by signal subspace approximation," *IEEE Trans. Signal Process.*, vol. 40, no. 12, pp. 2961–2972, Dec. 1992.
[32] G. Xu and T. Kailath, "Fast subspace decomposition," *IEEE Trans. Signal Process.*, vol. 42, no. 3, pp. 539–551, Mar. 1994.
[33] J. Liesen and Z. Strakos, *Krylov Subspace Methods: Principles and Analysis*. Oxford, U.K.: Oxford Univ. Press, 2013.
[34] J. W. Demmel, *Applied Numerical Linear Algebra*. Philadelphia, PA, USA: SIAM, 1997.
[35] S. M. Kay, *Fundamentals Statistical Signal Processing: Estimation Theory*. Upper Saddle River, NJ, USA: Prentice-Hall, 1993.
[36] T. Kazaz, G. J. M. Janssen, J. Romme, and A.-J. Van Der Veen, "Delay estimation for ranging and localization using multiband channel state information," *IEEE Trans. Wireless Commun.*, early access, Sep. 30, 2021, doi: 10.1109/TWC.2021.3113771.

SHAMMAN NOOR SHOUDHA (Student Member, IEEE) received the B.Sc. degree in electrical and electronics engineering from the Bangladesh University of Engineering and Technology, in 2017, and the M.Sc. degree in electrical engineering from The University of Texas at Dallas, in 2021, where he is currently pursuing the Ph.D. degree in electrical engineering. His current research interests include wireless localization and machine learning applications. He received the Louis Beecherl Jr. Graduate and the Phil Ritter Endowed Fellowships in 2021 and 2022, respectively.

JAYSON P. VAN MARTER (Student Member, IEEE) received the B.S. degree *(summa cum laude)* in electrical engineering from The University of Texas at Dallas, in 2020, where he is currently pursuing the Ph.D. degree with a focus in wireless information systems. During spring and summer 2020, he developed a USRP software-defined radio testbed engine as a TxACE Intern. His current research interests include real-time embedded systems, localization, millimeter-wave radar, terahertz radar, and SAR imaging algorithms. He received the TxACE Promising Researcher Award in May 2020 and the Jonsson School Excellence in Education Doctoral Fellowship in August 2020.

SHERIEF HELWA (Student Member, IEEE) received the B.S. and M.S. degrees from Ain Shams University, Cairo, Egypt, in 2012 and 2017, respectively. He is currently pursuing the Ph.D. degree in electrical engineering with The University of Texas at Dallas, Richardson, TX, USA. From 2014 to 2015, he was a Research Engineer with Alcatel-Lucent (acquired by Nokia) under Bell Labs org., where he worked on capacity dimensioning and RF planning algorithms and tools. From 2015 to 2018, he was developing signal processing algorithms and doing wireless system design with Axxcelera Broadband Wireless, Cairo. In 2019, he joined as an Intern with the Connectivity Department, Facebook Inc., Menlo Park, CA, USA, where he worked on the "Rural Access" Project. In 2020, he joined as an Intern Qualcomm Corporation, San Diego, CA, USA, and contributed to Qualcomm's 802.11ax access point design. His research interests include signal processing for digital communication systems and machine learning applications.

ANAND G. DABAK (Fellow, IEEE) received the bachelor's degree from the IIT, Bombay, India, in 1987, and the master's and Ph.D. degrees in electrical engineering from Rice University, in 1989 and 1992, respectively. He joined the DSP Systems Research and Development Center, TI, as a Member of Technical Staff working on wireless systems, in 1995. He worked until 2011 on algorithms, standards, systems issues related to communications, namely 3GPP, WCDMA, LTE, UWB, powerline communications (PLC), and modem development on TI processors. From 2011 to 2019, he worked with Kilby labs on ultrasonic flow metering for residential water and gas metering. From 2019 to 2021, he developed localization solutions for Bluetooth low energy (BLE) systems using both angle of arrival (AoA) and employed super resolution techniques for high accuracy distance measurement (HADM) phase-based techniques. Since 2021, he has been working in the radar group on applying signal processing techniques to radar applications. He has more than 250 patents in the areas of signal processing for wireless, PLC, and ultrasound application to flow metering. He has been a TI Fellow, since 2007.

MURAT TORLAK (Senior Member, IEEE) received the M.S. and Ph.D. degrees in electrical engineering from The University of Texas at Austin, in 1995 and 1999, respectively. Since August 1999, he has been with the Department of Electrical and Computer Engineering, The University of Texas at Dallas, where he has been promoted to the rank of a Full Professor. He is currently working as a Rotating Program Director of the U.S. National Science Foundation (NSF). His current research interests include experimental verification of wireless networking systems, cognitive radios, millimeter-wave automotive radars, millimeter-wave imaging systems, and interference mitigation in radio telescopes. He was the General Chair of Symposium on Millimeter Wave Imaging and Communications in 2013 IEEE GlobalSIP Conference. He has served as an Associate Editor for the IEEE TRANSACTIONS ON WIRELESS COMMUNICATIONS, from 2008 to 2013. He was a Guest Co-Editor of the IEEE JOURNAL OF SELECTED TOPICS IN SIGNAL PROCESSING Special Issue on Recent Advances in Automotive Radar Signal Processing in 2021.

NAOFAL AL-DHAHIR (Fellow, IEEE) received the Ph.D. degree from Stanford University. He was a Principal Member of Technical Staff at the GE Research Center and AT&T Shannon Laboratory, from 1994 to 2003. He is currently a Erik Jonsson Distinguished Professor with the ECE Department and the Associate Head at the UT-Dallas. He is the co-inventor of 43 issued patents and the coauthor of about 490 articles. He is a fellow of the National Academy of Inventors. He was a co-recipient of five IEEE best paper awards. He received the 2019 IEEE SPCC Technical Recognition Award and 2021 Qualcomm Faculty Award. From January 2016 to December 2019, he served as the Editor-in-Chief for the IEEE TRANSACTIONS ON COMMUNICATIONS.